HIGH-EFFICIENCY BACK-JUNCTION SILICON SOLAR CELL WITH AN IN-LINE EVAPORATED ALUMINUM FRONT GRID

M. Kessler[1], D. Münster[1], T. Neubert[1], C.P. Mader[1], J. Schmidt[1], and R. Brendel[1,2]
[1]Institute for Solar Energy Research Hamelin (ISFH), Am Ohrberg 1, 31860 Emmerthal, Germany
[2]Institute for Solid State Physics, University of Hannover, Appelstraße 2, 30167 Hannover, Germany

ABSTRACT

We present *n*-type silicon PERT (passivated emitter and rear totally diffused) solar cells with an Al_2O_3/SiN_x-passivated BBr_3-diffused back-junction emitter. The aluminum front side grid is evaporated in an industrial-type in-line evaporation system. The efficiency of the best 4 cm^2 solar cell is 19.6%, the fill factor is 79%, the open-circuit voltage is 660 mV and the short-circuit current density is 37.6 mA/cm^2. We use (700±10) µm-thick silicon shadow masks for the in-line evaporation of the aluminum front grid. The masks are fabricated by a laser process and subsequent anisotropic etching. The resulting finger width of the in-line evaporated fingers is (60±20) µm. The dynamic aluminum deposition rate is 5 µm×m/min for a carrier speed of 0.33 m/min. During in-line evaporation the linear thermal expansion of the mask is limited to (15±5) µm. Our n^+np^+-solar cell structure uses 2 high temperature diffusion processes: A P diffusion and a subsequent B diffusion. An essential element of our cell process is the order of these diffusions: We redistribute the phosphorus atoms of the front surface field during the subsequent high-temperature boron diffusion on the rear. The resulting phosphorus surface concentration is $(7±1)×10^{19}$ cm^3 and the corresponding sheet resistance is (80±10) Ω/□. A reference cell with a front grid statically evaporated in a laboratory-type reactor through a metal mask shows an efficiency of 20.4%. We thus confirm the high quality of the passivated boron back-junction emitter and of the efficiency potential of our solar cell structure.

INTRODUCTION

Phosphorus *n*-type Chochralski(Cz)-grown silicon features two important advantages over boron-doped Cz p-type silicon: A high minority carrier lifetime [1,2] and no degradation of the carrier lifetime due to boron-oxygen complexes [3].The liquid source BBr_3-diffusion process is widely spread within solar cell research. BBr_3-diffused p^+-type regions lead to the highest efficiencies reported so far for crystalline silicon solar cells [4,5,6]. Alternatives for forming a *pn*-junction on *n*-type silicon such as aluminum screen-printing [7] or boron-containing spin-on dielectrics [8] have been investigated. However, solar cell efficiencies were limited due to enhanced recombination [9]. A reduction in bulk lifetime when using a spin on dielectrics to form the B emitter required a subsequent high temperature P Diffusion to recover the bulk lifetime [8]. We therefore select the BBr_3-diffusion process for our cell structure.

The standard technology to form the semiconductor-metal contact in industrial solar cell production is screen printing. However, very shallow emitters that are required for high efficiencies are difficult to contact by screen printing without using selective emitters. Evaporation of Al is a possible alternative to screen printing that is compatible with shallow emitters. Twenty years back Schott Solar AG already used a batch-type system for aluminum evaporation in a solar cell pilot production line [10]. Since then, to the best of the author's knowledge, aluminum evaporation in industrial production of solar cells was only used for seed layer deposition and subsequent electroless plating [11]. In-line aluminum evaporation for the formation of a solar cell front grid was not yet investigated.

In this work we therefore investigate an in-line evaporation front grid concept. We apply this in-line-evaporated front contact grid to 4 cm^2-sized *n*-type silicon PERT solar cells with a full area BBr_3-diffused back junction emitter and a full area phosphorus-diffused front surface field (FSF). We chose a back junction cell as this cell type is sensitive to front recombination and any negative influence of the in-line-evaporated front grid strongly affects cell characteristics.

SILICON SHADOW MASKS FOR IN-LINE FRONT GRID EVAPORATION

We prepare silicon masks for in-line evaporation of the front grid: SiN_x is deposited on one side of a 700 µm-thick silicon wafer and the finger design is defined by using a disc laser (1030 nm, pulse duration 10^{-6} s) as is indicated in Fig. 1.

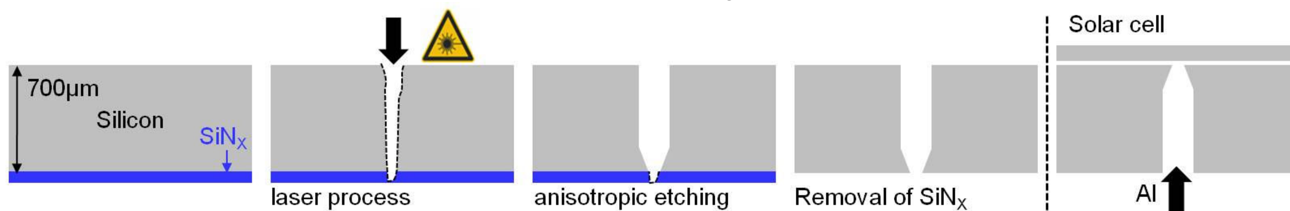

Figure 1 Preparation procedure of silicon shadow masks for in-line front grid evaporation of aluminum.

We etch the masks in a KOH solution to anisotropically remove the silicon within the laser induced openings. Finally the SiN_x is removed in hydrofluoric acid. The resulting geometry of the opening is indicated in Fig. 1 and Fig. 2 shows an SEM image of the silicon shadow mask after its use in an in-line evaporation system (ATON 500, Applied Materials).

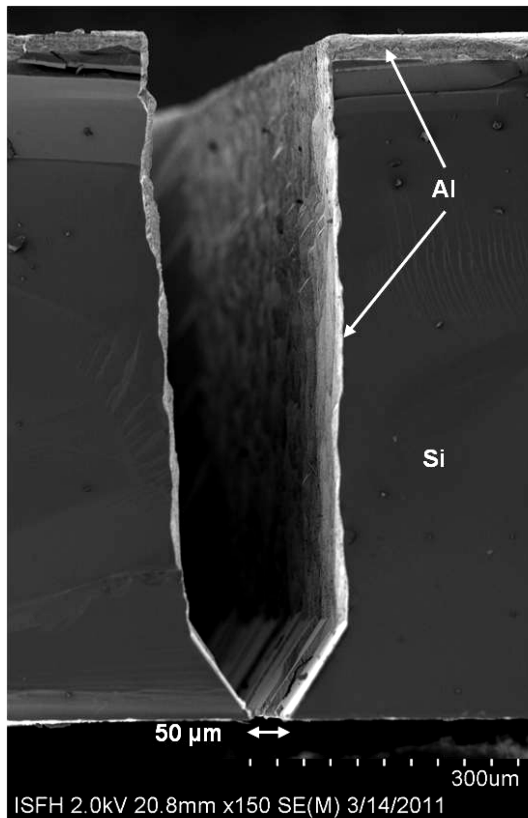

Figure 2 SEM micrograph of silicon shadow mask after in-line Al evaporation of the front grid.

Fig. 3 shows the resulting finger grid on a solar cell and a SEM micrograph of an in-line-evaporated finger. The resulting finger width of the in-line evaporated front grid is (60±20) µm and the corresponding finger height is (2±1) µm. In prior experiments we used one of these silicon masks for two subsequent in-line front grid evaporations on a planar test structures *without* removing the aluminum from the silicon mask in the meantime. The finger width remains constant for both evaporation sequences (60±5) µm and the finger height also remains unchanged (3±1) µm. For this reason we expect a multiple reusability of the mask. It needs to be investigated how often this mask is reusable. We simulate the temperature development of the Si-mask using an experimentally verified model [12].The peak temperature of the mask during the in-line front grid evaporation is (340±10) °C according to this simulation.

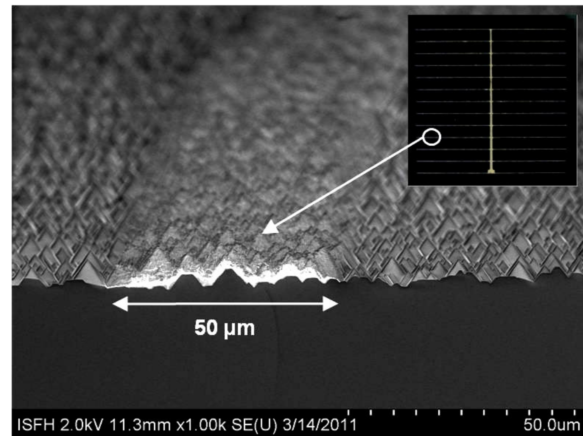

Figure 3 In-line evaporated front grid on solar cell and corresponding SEM micrograph of an in-line evaporated finger.

We determine the linear thermal expansion of the mask to be (17.5±0.5) µm for the simulated peak temperature. The bow of the masks during in-line evaporation defines the maximum gap between mask and solar cell. We calculate the gap between solar cell and mask using a simplified analytical bimetal correlation. For the simulated peak temperature the bow of our masks during in-line evaporation is (160±10) µm. We avoid any aluminum deposition outside the finger regions due to the small gap between mask and solar cell. Besides, an enhanced bow of the mask would not permit any reusability of the masks.

SOLAR CELL PROCESSING AND DESIGN

We fabricate 4 cm^2-sized *n*-type silicon PERT solar cells with a schematic cross section shown in Fig. 4. We use phosphorus-doped <100>-oriented 125x125mm^2 sized Cz silicon wafers of 300 to 305 µm starting thickness. The bulk resistivity of the *n*-type wafers is (2±0.5) Ωcm. The silicon wafers are etched to a thickness of (255±5) µm in a KOH solution. After a subsequent RCA cleaning step we perform a wet oxidation and define 21x21mm^2 windows with a laser (532 nm, pulse duration 10^{-12} s). We etch 3 µm of the silicon in KOH to remove the laser damage and the front side of the wafer is textured in a KOH-Isopropanol solution.

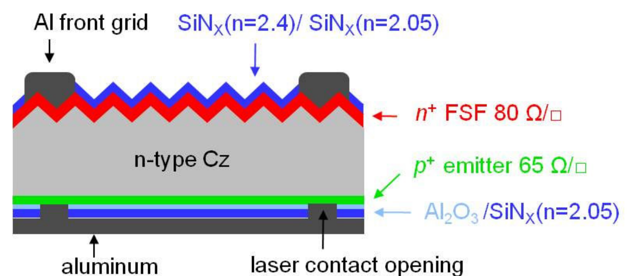

Figure 4 Schematic cross section of our PERT back-junction *n*-type silicon solar cells.

The samples are RCA-cleaned prior to the high temperature diffusion processes. We first perform the phosphorus diffusion and use the thermal budget of the subsequent boron diffusion process for redistributing the phosphorus atoms of the front surface field (FSF). The initial phosphorus $POCl_3$ diffusion process (75 min, 850°C) yields a sheet resistance of (65±5) Ω/□. The corresponding concentration profile is shown in Fig. 5 (red circles).

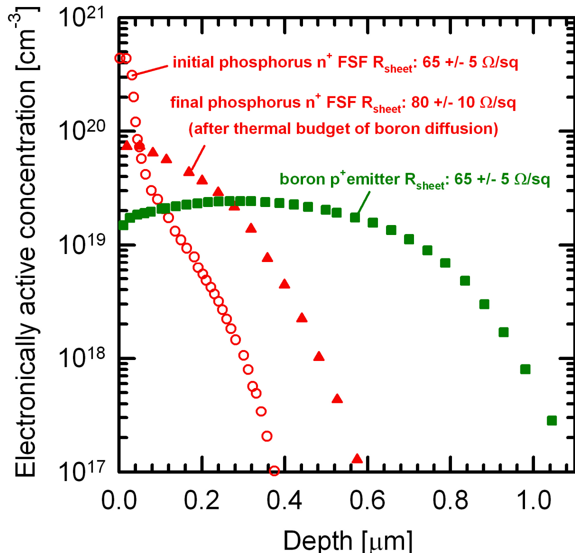

Figure 5 Doping profiles of the initial n^+-FSF (red circles) and the final n^+-FSF (red triangles) after the boron diffusion process. Profile of the p^+ back-junction emitter (green squares).

We deposit a 130 nm thick SiN_x layer on the textured n^+-type FSF to prevent any diffusion of boron atoms into the front surface. After an RCA cleaning step, the boron diffusion is carried out at 1000°C for 85 min and yields a sheet resistance of (65±5) Ω/□. Fig. 5 (green squares) shows the corresponding boron emitter profile measured with the electrochemical capacitance voltage (ECV) method [13]. The high temperature drive-in of the boron diffusion process includes a 60 min in-situ oxidation step. The oxygen reconverts a boron-rich layer (BRL) that forms at high temperatures during the BBr_3 diffusion processes to a boron silicate glass (BSG) [14]. The boron emitter profile features a junction depth of 1.1 μm. Thus we prevent any spiking of aluminum through the emitter during the full-area rear side aluminum evaporation. The high thermal budget of the boron diffusion process leads to a favorable distribution of phosphorus atoms: The phosphorus surface concentration decreases from $(4.5\pm0.5)\times10^{20}$ cm^{-3} to $(7\pm1)\times10^{19}$ cm^{-3} and the corresponding sheet resistance increases to (80±10) Ω/□ (red triangles in Fig. 5). This redistribution allows for a reduced recombination rate at the front side [15]. After the BBr_3 boron diffusion the BSG and the SiN_x is removed from all wafers using HF and the samples are cut into $25x25mm^2$ samples using a disc laser.

We passivate the rear-side boron emitter by Al_2O_3/SiN_x stacks [16], where the Al_2O_3 layer is grown at 225°C by plasma-assisted atomic layer deposition (plasma ALD) in a FlexAL™ reactor by Oxford Instruments. Plasma-enhanced chemical-vapor-deposited (PECVD) SiN_x (n=2.05, 120 nm) is deposited at 400°C onto the Al_2O_3 layer in a PlasmaLab 80+ reactor (Oxford Instruments) as a capping layer. The SiN_x deposition temperature is sufficient to activate the surface passivation of the Al_2O_3 layer [17]. We investigate if any additional annealing is required to further improve the passivation quality. We therefore prepare symmetrical p^+np^+ test structures with an identical Al_2O_3/SiN_x double layer passivation stack and identical silicon base as used for our solar cells. We anneal these test structures on a hotplate at 400 °C for 5 and 15 min. We measure the respective effective carrier lifetime with the WCT 120 Sinton lifetime tester before and after the annealing steps. Fig. 6 shows the Auger-corrected inverse effective carrier lifetime as a function of the average excess carrier density Δn of our passivated symmetrical p^+np^+ test structures. We use the Auger-correction as implemented into the WCT 120 evaluation spreadsheet. We use the Kane & Swanson [18] approach for symmetrical samples to extract the corresponding emitter saturation current densities (J_{0E}) using an intrinsic carrier concentration of $n_i=10^{10}cm^{-3}$.

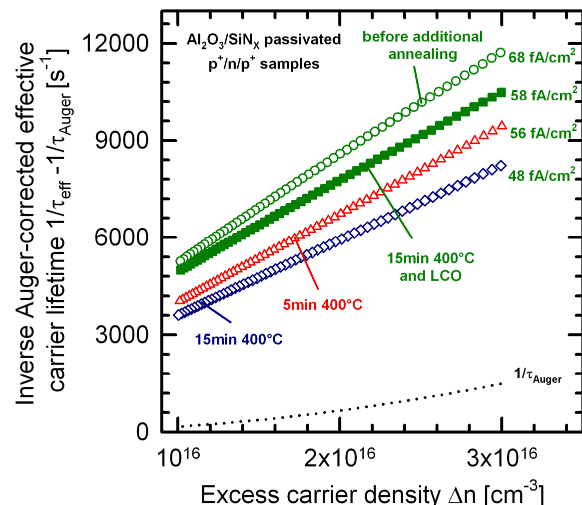

Figure 6 Inverse Auger-corrected effective carrier lifetime of p^+np^+ samples before (green circles) and after annealing (red triangles, blue diamonds) as well as after subsequent laser contact opening (green squares).

The J_{0E}–value decreases from initially 68 fA/cm^2 to 48 fA/cm^2 after 15 min of annealing at 400°C. For further annealing at 400°C the lifetime remains constant (not shown in Fig. 6). The thermal budget during front and rear side SiN_x capping layer deposition at 400°C already activated the Al_2O_3 passivation (green circles in Fig. 6). Note that our solar cells experience a different thermal budget after Al_2O_3 deposition compared to our symmetrical

lifetime test structures because (1) there is only *one* SiN_x capping layer deposition at 400°C and (2) an SiN_x double layer is deposited on the front at 400°C. To further improve the passivation quality of the Al_2O_3/SiN_x stack on the p^+ emitter, we anneal our solar cells on a hotplate for 10 min at 425°C prior to further cell processing.

Subsequently, we evaporate two different aluminum front side grids prior to front side passivation of the front side and the rear side metallization:

1. The in-line front grid, evaporated within the industrial-type in-line evaporation system ATON 500 (Applied Materials). The pitch of the Al fingers is 1.66mm and the finger width is (60±20) µm. The overall shading is 4.55% (finger shading: 3.3%). We evaporate the in-line front grid onto all solar cells in one run using a batch of the silicon masks described above.
2. A laboratory front grid using Ni shadow masks in a laboratory evaporation system is used for reference purposes. The pitch of the fingers is 1.05 mm and the finger width is (20±10) µm. The overall shading is 3.4% (finger shading: 2.7%).

After aluminum front side metallization the n^+ FSF is passivated with a SiN_x(n=2.4) /SiN_x(n=2.05) double layer deposited at 400°C which also serves as antireflection coating. The J_{0E} value of an identically passivated n^+nn^+ test structure is 110 fA/cm^2. The J_{0E} determination is performed as described above for the n^+pn^+ test structures. A line geometry with a pitch of 1.5 mm is opened at the rear side using a laser (532 nm, pulse duration 10^{-12}s). The opened area fraction is approximately 3%. The inverse Auger-corrected lifetime of a p^+np^+ test structure after annealing and laser contact opening (LCO) of the dielectric layer on both sides of the symmetrical sample is included in Fig. 6 (green squares). The extracted J_{0E} after LCO is 58 fA/cm^2. The emitter current density within the LCO regions $J_{0E,LCO}$ is (350±25) fA/cm^2 for the opened area fraction of 3%. Finally, we deposit 2 µm of Aluminum on the rear side of the cell by in-line evaporation using the ATON500 system. We anneal all solar cells prior to cell characterization on a hotplate at 300°C for 1 minute to improve the rear contact.

SOLAR CELL RESULTS AND DISCUSSION

Table 1 shows the cell parameters of our solar cells with the respective front grid. The average efficiency with in-line evaporated front grid is 19.4% and the corresponding low standard deviation indicates a good stability of the mask preparation process and the in-line aluminum evaporation process. The table shows the data of all fabricated solar cells from one run. The low average fill factor (*FF*) of 78.9 % is partly due to an enhanced series resistance caused by the only (2±1) µm-thick fingers. Another cell run with in-line evaporated fingers having (5±2) µm-thick fingers shows a *FF* = 80.4 %. Furthermore the large finger pitch of 1.66mm leads to an increased internal series resistance when compared to the reference process that has a pitch of only 1.05 mm. Our 2D simulations using the conductive boundary model [19] show that the *FF* increases by 0.3 to 0.4% due to the increased finger pitch. We explain the rather low short-circuit current density of J_{SC} = 37.6 mA/cm^2 and 38.5 mA/cm^2 for both cell types by recombination at the n^+-type FSF. The internal quantum efficiency (IQE) at a wavelength of 350 nm is 0.66±0.01 for the laboratory front grid and 0.64±0.01 for the in-line-evaporated front grid. Bock et al. [7] showed an IQE value of 0.8 at a wavelength of 350 nm using a 250 Ω/□ FSF. This comparison indicates that the currently used n^+-type phosphorus FSF is not yet optimized.

The limit of the open-circuit voltage $V_{OC,limit}$ can be calculated by

$$V_{OC,\,limit} = \frac{kT}{q} \cdot ln\left(\frac{J_{SC}}{J_{0E,\,rear} + J_{0E,\,front} + J_{0,bulk}} + 1\right) \qquad (1)$$

where kT/q=0.257 V (25 °C). $J_{0E,rear}$ and $J_{0E,front}$ are the area-weighted saturation current densities from passivated and metalized regions at the front and rear side, respectively.

Table 1 Short-circuit current density J_{SC}, open-circuit voltage V_{OC}, fill factor *FF* and efficiency *η* of our solar cells with in-line evaporated and laboratory front grid, respectively (in-house measurement, 100mW/cm^2, 25 ± 0.1°C). The corresponding standard deviation of the average cell parameters is shown in brackets.

	Area [cm^2]	J_{SC} [mA/cm^2]	V_{OC} [mV]	*FF* [%]	*η* [%]
In-line evaporated front grid (best)	**4**	**37.6**	**660.0**	**79**	**19.6**
In-line evaporated front grid (average of 5)	4	37.3 (0.2)	659.0 (0.7)	78.9 (0.2)	19.4 (0.14)
Laboratory front grid (best)	**4**	**38.5**	**662.3**	**79.9**	**20.4**
Laboratory front grid (average of 6)	4	38.3 (0.3)	661.3 (1.4)	79.8 (0.3)	20.2 (0.2)

The contacted area on the front side is 4.55% for the in-line-evaporated and 3.4% for laboratory cell. The contacted area at the rear is 3% for both cell types. The average J_{SC} is 37.3 mA/cm^2 and 38.3 mA/cm^2. The respective J_{0E} from the passivated regions is 48 fA/cm^2 (rear boron emitter, see Fig. 6) and 110 fA/cm^2 (phosphorus FSF). We assume a saturation current density of 350 fA/cm^2 in the metalized regions at the rear and 700 fA/cm^2 in the metalized regions at the front. Any bulk recombination is neglected. The calculated $V_{OC,limit}$ is 667.6 mV for the cell with the in-line evaporated and 669.2 mV for the cell with laboratory front grid. The difference in open-circuit voltages is 2.3 mV (measurement) and 1.6 mV (calculation). This qualitative consistent offset in V_{OC} results from the enhanced metallization fraction of the in-line-evaporated cells. The deviation of calculated and measured V_{OC} can be explained by either bulk recombination or by the inaccuracy of the assumed emitter current densities within the metalized areas. Furthermore, the intrinsic carrier concentration n_i that is used for J_{0E} extraction influences the calculated $V_{OC,limit}$.

SUMMARY

We have presented PERT *n*-type silicon solar cells with an in-line evaporated front grid and an Al_2O_3/SiN_x-passivated boron-diffused rear emitter. Using this cell type, we have demonstrated open-circuit voltages of 660 mV and efficiencies up to 19.6%. The front grid of these cells was evaporated in an industrial inline system using silicon shadow masks which allow obtaining a finger width of (60±20) µm. Identically processed solar cells with laboratory-type evaporated front grid showed an efficiency of 20.4%. Additionally, we pointed out the positive impact of the following process steps: (i) We used the thermal budged of the boron diffusion to achieve a favorable redistribution of the n^+ phosphorus FSF. (ii) The thermal budget of the SiN_x capping layer deposition and the front side SiN_x passivation was demonstrated to be suitable to replace the required annealing step for boron emitter passivation using ALD-Al_2O_3.

ACKNOWLEDGMENT

Funding was provided by the State of Lower Saxony and the German Ministry for the Environment, Nature Conservation and Nuclear Safety (BMU) under contract numbers 0325050 and 0325195A.

REFERENCES

[1] A. Cuevas, M. Kerr, C. Ferrazza, and G. Coletti, *Appl.Phys. Lett*. **81**, 2002, 4952.

[2] D. MacDonald and L.J. Gerlings, *Appl. Phys. Lett*. **85 ,** 2004, pp. 4061-63.

[3] K. Bothe, R. Sinton, and J. Schmidt, *Prog. Photovoltaics* **13,** 2005, 287.

[4] J. Zhao, A. Wang and M.A.Green, Prog. Photovolt: Res. Appl. 7, 1999, pp. 471-474.

[5] J. Benick, A. Richter, T.T.A. Li, N.E. Grant, K.R. McIntosh, Y. Ren, K.J. Weber, M. Hermle, S.W. Glunz, Proc. 35th IEEE Photovoltaic Specialist Conference, Honolulu, Hawaii, 2010, pp. 891-896.

[6] P.J. Cousins, D.D. Smith, H.-C. Luan, J. Manning, T. D. Dennis, A. Waldhauer, K.E. Wilson, G. Harley, W. P. Mulligan, Proc. 35th IEEE Photovoltaics Specialists Conference, Honolulu, Hawaii, 2010, pp. 823-826.

[7] R. Bock, J. Schmidt, S. Mau, B. Hoex, E. Kessels, R. Brendel, Proc. 34th IEEE Photovoltaics Specialists Conference, Philadelphia, Pensylvania, 2009, pp. 30-35.

[8] A. Das, D.S. Kim, K. Nakayashiki, B. Rounsaville, V. Meemongkolkiat, *Journal of The Electrochemical Society,* **157**, 6, 2010, H684-H687.

[9] R. Bock, J. Schmidt, P.P. altermatt, R. Brendel, Semicond. Sci. Technol. **25**, 10**,** 105007, 2010.

[10] R. Hezel, W. Hoffmann and K. Jaeger, Proc. 10th European Photovoltaic Solar Energy Conference, 1991, pp. 511-514.

[11] T. Bruton, M. Mason, S. Roberts, O. Hartley, S. Gledhill, O. Fernandez, R. Russel, W. Warta, S. Glunz, O. Schulz, M. Hermle, G. Willeke, Proc. 3rd World Conference on Photovoltaic Energy Conversion, Osaka, Japan, 2003.

[12] C. Mader, M. Kessler, U. Eitner, R. Brendel, "Temperature of silicon wafers during in-line high-rate evaporation of Aluminum", submitted to Solar Energy Materials and Solar Cells, 2011.

[13] E. Peiner, A. Schlachetzki, D. Krüger, *J. Electrochem. Soc.* **142**, 1995, pp. 576-580.

[14] M. Kessler, T. Ohrdes, B. Wolpensinger, N.-P. Harder, Semicond. Sci. Technol. **25**, 5**,** 055001, 2010.

[15] A. Cuevas, P.A. Basore, G. Giroult-Matlakowski, C. Dubois, *J. Appl. Phys.* **80**, 1996, 3370.

[16] J. Schmidt, B. Veith, and R. Brendel, "Effective surface passivation of crystalline silicon using ultrathin Al_2O_3 films and Al_2O_3/SiN_x stacks", Phys. Status Solidi RRL **3**, 287-289 (2009).

[17] B. Veith, F. Werner, D. Zielke, R. Brendel, J. Schmidt, Comparison of the thermal stability of single Al_2O_3 layers

and Al_2O_3/SiN_x stacks for the surface passiviation of silicon, Energy Procedia, 2011, in press.

[18] D.E. Kane and R.M. Swanson, in Proceedings of the 18th IEEE PVSC (IEEE, New York, 1985), p. 578.

[19] S. Eidelloth, U. Eitner, S. Steingrube, R. Brendel, in Proc of 25th European Photovoltaic Solar Energy Conference, Valencia, 2010.